Inorg. Chem. **2005**, *44*, 8822–8835

From Low-Dimensional Manganese(II) Azido Motifs to Higher-Dimensional Materials: Structure and Magnetic Properties

En-Qing Gao,*,† Ai-Ling Cheng,† Yan-Xia Xu,† Ming-Yuan He,† and Chun-Hua Yan‡

Shanghai Key Lab of Green Chemistry and Chemical Processes, Department of Chemistry, East China Normal University, Shanghai 200062, China, and State Key Lab of Rare Earth Materials Chemistry and Applications, Peking University, Beijing 100871, China

Received July 24, 2005

Four new inorganic–organic hybrid coordination polymers in which 1D or 2D manganese(II) azido inorganic motifs are interlinked into higher-dimensional networks have been synthesized by use of a series of bis(pyridyl)-type organic bridging ligands (linkers) with different side groups and/or different coordination orientations. The dimensionality and the topology of the manganese(II) azido motif and the whole structure are sensitive to the organic linkers used. Compounds **1** and **3** are 3D coordination polymers with pillared-layer architectures: in **1**, 2D Mn(II) layers with alternate double end-on (EO) and single end-to-end (EE) azido bridges are pillared by zigzag organic linkers, and **3** is built from single EE azido-bridged Mn(II) layers and linear organic linkers. The 3D nets of **1**, **3**, and related compounds have been related to the specific length and coordination orientation of the organic pillars and the undulate shape of the manganese(II) azido layers. Consistent with their structures, both **1** and **3** exhibit weak ferromagnetism due to spin canting. Compound **1** is a weak ferromagnet with $T_c = 16$ K, and **3** is a metamagnet with $T_c = 23$ K. On the other hand, compounds **2** and **4** are 2D coordination networks in which 1D manganese(II) azido chains are interlinked by organic linkers: **2** is the first 2D network built from Mn(II) chains with alternate double EE and double EO azido bridges, which mediate antiferro- and ferromagnetic interactions, respectively; **4** is the first 2D network built from Mn(II) chains with only single EE azido bridges, which mediate antiferromagnetic interactions. The magnetic susceptibility of **4** exhibits a rapid rise at very low temperature, which may be attributed to paramagnetic impurities or spin canting.

Introduction

The design of molecular magnetic materials, such as molecular ferromagnets and single-molecule magnets, has been of considerable interest in recent years.[1,2] The basic strategy to design such materials is to organize paramagnetic centers into polynuclear or polymeric aggregates by use of bridging ligands that can efficiently propagate magnetic superexchange. The bulk magnetic properties depend on the nature and magnitude of the superexchange propagated by the bridge, the extended bridging networks, and the cooperative interactions between the magnetic aggregates, besides the nature of the metal ions. As a versatile bridging ligand and efficient superexchange mediator, the pseudohalide azido ion is among those that have evoked the most intense attention.[3−10] The azido ion can link metal ions in μ-1,1 (end-on, EO), μ-1,3 (end-to-end, EE), μ-1,1,3, or still other modes,[3,4] and the magnetic exchange mediated via an azido bridge can be ferro- (F) or antiferromagnetic (AF), depending on the bridging mode and structural parameters of the bridging moiety. Besides discrete binuclear and polynuclear

* To whom correspondence should be addressed. E-mail: eqgao@chem.ecnu.edu.cn. Fax: +86-21-62233424.

† East China Normal University.

‡ Peking University.

(1) (a) Kahn, O. *Molecular Magnetism*; VCH: New York, 1993. (b) Miller, J. S., Drilon, M., Eds. *Magnetism: Molecules to Materials*; Wiley-VCH: Weinheim, Germany, 2002.

(2) Gatteschi, D.; Sessoli, R. *Angew. Chem., Int. Ed.* **2003**, *42*, 268−297.

(3) Ribas, J.; Escuer, A.; Monfort, M.; Vicente, R.; Cortés, R.; Lezama, L.; Rojo, T. *Coord. Chem. Rev.* **1999**, *193−195*, 1027 and references cited therein.

(4) For examples, see: (a) Mialane, P.; Dolbecq, A.; Marrot, J.; Rivière, E.; Sécheresse, F. *Chem.—Eur. J.* **2005**, *11*, 1771−1778 (μ-1,1,1,3,3,3). (b) Goher M. A. S.; Cano, J.; Journaux, Y.; Abu-Youssef, M. A. M.; Mautner, F. A.; Escuer, A.; Vicente, R. *Chem.—Eur. J.* **2000**, *6*, 778−784 (μ-1,1,1). (c) Ribas, J.; Montfort, M.; Solans, X.; Drillon, M. *Inorg. Chem.* **1994**, *33*, 742−745 (μ-1,1,3). (d) Papaefstathiou, G. S.; Perlepes, S. P.; Escuer, A.; Vicente, R.; Font-Bardia, M.; Solans, X. *Angew. Chem., Int. Ed.* **2001**, *40*, 884−886 (μ-1,1,1,1). (e) Meyer, F.; Kircher, P.; Pritzkow, H. *Chem. Commun.* **2003**, 774−775 (μ-1,1,3,3).

10.1021/ic0512328 CCC: $30.25
Published on Web 10/13/2005

molecules,[5] an increasing number of coordination polymers[6−8] with extended TM azido (TM = paramagnetic transition-metal ions) networks have been synthesized, and they exhibit a great diversity of structural motifs and magnetic properties. Besides several TM azido polymers without any coligands,[4b,8] most species contain organic coligands, and a minor change in the coligands may lead to significant changes in the azido bridging mode, the dimensionality, and the topology of the TM azido network. The observed bulk magnetic behaviors include antiferromagnetism, ferromagnetism, ferrimagnetism, metamagnetism, weak ferromagnetism related to spin canting, and paramagnetism.

In disproportion with the large number of known one-(1D)[6] and two-dimensional (2D)[7] TM−azido coordination polymers, three-dimensional (3D) networks are limited, with known examples including $A_n[Mn(N_3)_3]_n$ ($A = Cs^+$ [4b] and Me_4N^+ [8]) and $[Mn(N_3)_2(py)_2]_n$.[9] An interesting approach to 3D motifs is to incorporate bis(pyridyl)-derived organic bridging ligands into the TM(II) azido systems, although this approach has succeeded in only a few cases: (i) 3D TM(II) azido networks have been generated by incorporating pyridazine (TM = Mn)[10] and 4,4′-bipyridine (TM = Mn, Fe),[11] which stabilize the 3D structures but do not lead to dimensional increase; (ii) the use of 2.2′-bipyrimidine,[12] pyrimidine,[10] or pyrazine-*N*,*N*′-dioxide[13] yielded 3D motifs in which 2D inorganic manganese(II) azido layers are interlinked by the organic ligands; (iii) recently, 1D manganese(II) azido chains have also been joined into 3D motifs by a bis(bidentate) bridging ligand.[14] It is noted that the approach failed to give 3D networks for many related organic linkers, such as pyrazine,[15] 4,4′-bipyridine dioxide,[16a] 4,4′-bipyridylethene,[16] 4,4′-bipyridylethane,[17] 4,4′-bipyridylpropane,[17b] and a series of open-chain diazine ligands containing two bidentate binding sites,[18] for which only 2D or even 1D structures were obtained. Nevertheless, these results demonstrated that the metal azido networks could be tuned by the organic cobridges. In particular, the success in building 3D magnets from 1D or 2D TM(II) azido motifs opens the possibility of tuning the interchain or interlayer interactions, and hence the bulk magnetic properties, by changing the length and geometry of the organic linkers.

Chart 1. Chemical Structures of the Organic Bridging Ligands Used

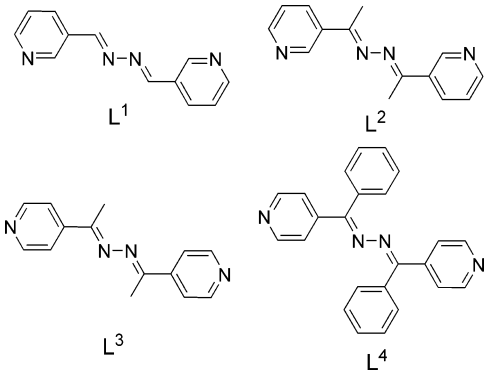

With these in mind, here we report the structures and magnetic properties of four manganese(II) azido coordination polymers assembled using a series of relatively long and semirigid bis(pyridyl) Schiff bases as organic linkers (L^1−L^4; Chart 1). With L^1 and L^3, we succeeded in obtaining two novel 3D networks in which 2D manganese(II) azido layers are pillared by the organic linkers: $[Mn(N_3)_2(L^1)]_n \cdot nH_2O$ (**1**) is built of (6,3) layers containing alternate double EO and single EE azido bridges, and $[Mn(N_3)_2(L^3)]_n$ (**3**) contains (4,4) grid layers with single EE azido bridges. The 3D nets of **1** and **3** are novel and different from those for related compounds reported previously. Because of spin canting within the manganese(II) azido layers, **1** behaves as a weak ferromagnet and **3** as a metamagnet with a large canting angle. On the other hand, the use of L^2 and L^4 afforded two different 2D coordination polymers in which manganese(II) azido chains are interlinked by the organic

(5) For recent examples, see: (a) Escuer, A.; Font-Bardía, M.; Massoud, S. S.; Mautner, F. A.; Peñalba, E.; Solans, X.; Vicente, R. *New J. Chem.* **2004**, *28*, 681−686. (b) Serna, Z. E.; Lezama, L.; Urtiaga, M. K.; Arriortua, M. I.; Barandika, M. G. B.; Cortés, R.; Rojo, T. *Angew. Chem., Int. Ed*. **2000**, *39*, 344−347. (c) Koner, S.; Saha, S.; Mallah, T.; Okamoto, K. *Inorg. Chem.* **2004**, *43*, 840−842. (d) Ray, M. S.; Ghosh, A.; Chaudhuri, S.; Drew, M. G. B.; Ribas, J. *Eur. J. Inorg. Chem.* **2004**, 3110−3117.

(6) For recent examples, see: (a) Gao, E.-Q.; Bai, S.-Q.; Yue, Y.-F.; Wang, Z.-M.; Yan, C.-H. *Inorg. Chem*. **2003**, *42*, 3642−3648 and references cited therein. (b) Gao, E.-Q.; Bai, S.-Q.; Wang, C.-F.; Yue, Y.-F.; He, Z.; Yan, C.-H. *Inorg. Chem*. **2003**, *42*, 8456−8464. (c) Ray, U.; Jasimuddin, Sk.; Ghosh, B. K.; Monfort, M.; Ribas, J.; Mostafa, G.; Lu, T.-H.; Sinha, C. *Eur. J. Inorg. Chem.* **2004**, 250−259. (d) Hong, C. S.; Koo, J.; Son, S.-K.; Lee, Y. S.; Kim, Y.-S.; Do, Y. *Chem. Eur. J*. **2001**, *7*, 4243−4252. (e) Abu-Youssef, M. A. M.; Escuer, A.; Goher, M. A. S.; Mautner, F. A.; Reiss, G.; Vicente, R. *Angew. Chem., Int. Ed.* **2000**, *39*, 1624−1626.

(7) For recent examples, see: (a) Gao, E.-Q.; Yue, Y.-F.; Bai, S.-Q.; He, Z.; Yan, C.-H. *Chem. Mater.* **2004**, 1590−1596 and references cited therein. (b) Shen, Z.; Zuo, J.-L.; Gao, S.; Song, Y.; Che, C.-M.; Fun, H.-K.; You, X.-Z. *Angew. Chem., Int. Ed*. **2000**, *39*, 3633−3635. (c) Goher, M. A. S.; Abu-Youssef, M. A. M.; Mautner, F. A.; Vicente, R.; Escuer, A. *Eur. J. Inorg. Chem.* **2000**, 1819−1823.

(8) (a) Mautner, F. A.; Cortés, R.; Lezama, L.; Rojo, T. *Angew. Chem., Int. Ed. Engl.* **1996**, *35*, 78−80. (b) Mautner, F. A.; Hanna, S.; Cortés, R.; Lezama, L.; Barandika, M. G.; Rojo, T. *Inorg. Chem.* **1999**, *38*, 4647−4652.

(9) Escuer, A.; Vicente, R.; Goher, M. A. S.; Mautner, F. A. *Inorg. Chem.* **1996**, *35*, 6386−6391.

(10) Escuer, A.; Vicente, R.; Goher, M. A. S.; Mautner, F. A.; Abu-Youssef, M. A. M. *Chem. Commun.* **2002**, 64−65.

(11) (a) Han, S.; Manson, J. L.; Kim, J.; Miller, J. S. *Inorg. Chem.* **2000**, *39*, 4182−4185. (b) Martin, S.; Barandika, M. G.; Lezama, L.; Pizarro, J. L.; Serna, Z. E.; de Larramendi, J. I. R.; Arriortua, M. I.; Rojo, T.; Cortés, R. *Inorg. Chem.* **2001**, *40*, 4109−4115. (c) Fu, A. H.; Huang, X. Y.; Li, J.; Yuen, T.; Lin, C. L. *Chem.*−*Eur. J.* **2002**, *8*, 2239−2247.

(12) De Munno, G.; Julve, M.; Viau, G.; Lloret, F.; Faus, J.; Viterbo, D. *Angew. Chem., Int. Ed. Engl.* **1996**, *35*, 1807−1810.

(13) Ma, B.-Q.; Sun, H.-L.; Gao, S.; Su, G. *Chem. Mater*. **2001**, *13*, 1946−1948.

(14) Liu, C.-M.; Gao, S.; Zhang, D.-Q.; Huang, Y.-H.; Xiong, R.-G.; Liu, Z.-L.; Jiang, F.-C.; Zhu, D.-B. *Angew. Chem., Int. Ed.* **2004**, *43*, 990−994.

(15) (a) Manson, J. L.; Arif, A. M.; Miller, J. S. *Chem. Commun.* **1999**, 1479−1480. (b) Hao, X.; Wei, Y.; Zhang, S. *Chem. Commun.* **2000**, 2271−2272.

(16) (a) Ghosh, A. K.; Ghoshal, D.; Zangrando, E.; Ribas, J.; Chaudhuri, N. R. *Inorg. Chem.* **2005**, *44*, 1786−1793. (b) Hong, C. S.; Son, S.-K.; Lee, Y. S.; Jun, M.-J.; Do, Y. *Inorg. Chem.* **1999**, *38*, 5602−5610.

(17) (a) Hernández, M. L.; Barandika, M. G.; Urtiaga, M. K.; Cortés, R.; Lezama, L.; Arriortua, M. I. *J. Chem. Soc., Dalton Trans.* **2000**, 79−84. (b) Konar, S.; Zangrando, E.; Drew, M. G. B.; Mallah, T.; Ribas, J.; Chaudhuri, N. R. *Inorg. Chem.* **2003**, *42*, 5966−5973.

(18) (a) Gao, E.-Q.; Bai, S.-Q.; Wang, Z.-M.; Yan, C.-H. *J. Am. Chem. Soc.* **2003**, *125*, 4984. (b) Gao, E.-Q.; Yue, Y.-F.; Bai, S.-Q.; He, Z.; Yan, C.-H. *J. Am. Chem. Soc.* **2004**, *126*, 1419−1429.

Table 1. Summary of Crystallographic Data for the Complexes

	1	2	3	4
formula	$C_{12}H_{12}MnN_{10}O$	$C_{14}H_{14}MnN_{10}$	$C_{14}H_{14}MnN_{10}$	$C_{25}H_{22}MnN_{10}O$
fw	367.26	377.29	377.29	532.46
T, K	293	293	293	293
crystal system	monoclinic	triclinic	monoclinic	monoclinic
space group	$C2/c$	$P\bar{1}$	$P2_1/c$	$C2/c$
a, Å	27.8153(5)	8.6051(7)	12.5610(7)	23.9365(5)
b, Å	8.6615(2)	8.6212(8)	8.5159(4)	10.8608(2)
c, Å	15.2390(3)	11.8163(11)	8.2206(4)	19.7789(5)
α, deg		104.866(4)		
β, deg	103.6010(10)	104.968(4)	105.093(2)	94.2343(7)
γ, deg		94.773(4)		
V, Å^3	3568.46(13)	807.96(12)	849.01(7)	5127.88(19)
Z	8	2	2	8
D_c, g cm^{-3}	1.367	1.551	1.476	1.379
μ(Mo Kα), mm^{-1}	0.761	0.838	0.798	0.554
θ range, deg	3.43−27.43	3.50−27.50	3.51−27.43	3.40−27.52
unique reflns/R_{int}	4027/0.0710	3570/0.0614	1890/0.0719	5827/0.0535
params refined	223	228	117	340
R1[a] [$I > 2\sigma(I)$]	0.0591	0.0427	0.0452	0.0664
wR2[b] (all data)	0.1813	0.1220	0.1239	0.1973

[a] $R1 = \sum||F_o| - |F_c||/\sum|F_o|$. [b] $wR2 = \{\sum[w(F_o^2 - F_c^2)^2]/\sum[w(F_o^2)^2]\}^{1/2}$.

linkers: the chain in complex $[Mn(N_3)_2(L^2)]_n$ (**2**) is built by alternate double EE and double EO azido bridges, which mediate AF and F interactions, respectively; $[Mn(N_3)_2(L^4)(CH_3OH)]_n$ (**4**) contains uniform chains with only single EE azido bridges, which mediate AF interactions. The preliminary results for **3** have been communicated elsewhere.[19]

Experimental Section

Materials and Synthesis. All of the starting chemicals were of analytical reagent grade and were used as received. The L^i ligands were prepared by the condensation reactions of the appropriate aldehyde or ketones with hydrazine according to literature procedures.[20]

Caution! *Although not encountered in our experiments, azido and perchlorate compounds of metal ions are potentially explosive. Only a small amount of the materials should be prepared, and it should be handled with care.*

$[Mn(L^1)(N_3)_2]_n \cdot nH_2O$ (1). A solution of manganese(II) perchlorate (0.4 mmol) and sodium azide (0.9 mmol) in water (5 mL) was mixed with a solution of L^1 (0.4 mmol) in methanol (15 mL), resulting in a clear yellow solution. Slow evaporation of the solution at room temperature yielded yellow crystals of **1** within 1 week. The crystals were collected by filtration, washed by methanol, and dried in air. Yield: 62%. Elem anal. Calcd (%) for $C_{12}H_{12}MnN_{10}O$: C, 39.25; H, 3.29; N, 38.14. Found: C, 39.38; H, 3.21; N, 37.76. IR (cm^{-1}, KBr): ν(O−H) 3440m, $\nu_{as}(N_3)$ 2100s, 2075s, ν(C═N) 1629m.

$[Mn(L^2)(N_3)_2]_n$ (2). Crystals of **2** were obtained by a procedure similar to that for **1**, using L^2 instead of L^1. Yield: 57%. Elem anal. Calcd (%) for $C_{14}H_{14}MnN_{10}$: C, 44.57; H, 3.74; N, 37.13. Found: C, 44.50; H, 3.56; N, 36.92. IR (cm^{-1}, KBr): $\nu_{as}(N_3)$ 2083s, ν(C═N) 1614m.

$[Mn(L^3)(N_3)_2]_n$ (3). Crystals of **3** were obtained by a procedure similar to that for **1**, using L^3 instead of L^1. Yield: 65%. Elem anal. Calcd (%) for $C_{14}H_{14}MnN_{10}$: C, 44.57; H, 3.74; N, 37.13. Found: C, 44.67; H, 3.61; N, 37.54. IR (cm^{-1}, KBr): $\nu_{as}(N_3)$ 2076s, ν(C═N) 1608m.

$[Mn(N_3)_2(L^4)(CH_3OH)]_n$ (4). A solution of manganese(II) perchlorate (0.2 mmol) and sodium azide (0.4 mmol) in methanol (15 mL) was mixed with a suspension of L^4 (0.2 mmol) in methanol (15 mL). The mixture was refluxed under stirring for 20 min to give a clear solution, which was cooled and filtered. Slow evaporation of the filtrate at room temperature afforded yellow crystals of **4**. Yield: 54%. Elem anal. Calcd (%) for $C_{25}H_{22}MnN_{10}O$: C, 56.29; H, 4.16; N, 26.26. Found: C, 55.99; H, 3.95; N, 26.18. IR (cm^{-1}, KBr): ν(O−H) 3372m, $\nu_{as}(N_3)$ 2121s, 2096s, 2053s, ν(C═N) 1611m.

Physical Measurements. Elemental analyses (C, H, N) were performed on an Elementar Vario EL analyzer. IR spectra were recorded on a Nicolet Magna-IR 750 spectrometer equipped with a Nic-Plan microscope. Temperature- and field-dependent magnetic measurements were carried out on an Oxford MagLab 2000 magnetometer. Diamagnetic corrections were made with Pascal's constants.

Crystallographic Studies. Diffraction intensity data for single crystals were collected at room temperature on a Bruker Smart Apex (for **1**) or a Nonius Kappa (for **2**−**4**) CCD area detector equipped with graphite-monochromated Mo Kα radiation ($\lambda = 0.710\ 73$ Å). Empirical absorption corrections were applied using the SADABS[21] (**1**) or Sortav[22] (**2**−**4**) program. The structure was solved by the direct method and refined by the full-matrix least-squares method on F^2 with anisotropic thermal parameters for all non-hydrogen atoms.[23] The water molecule in **1** exhibits disorder over two positions, for which the occupancies were refined to be 0.61 versus 0.39, and the water hydrogen atoms were not located. Hydrogen atoms were located geometrically and refined using the riding model, except for the hydroxyl hydrogen atom of the methanol molecule in **4**, which was located from the difference map. Pertinent crystallographic data and refinement parameters are summarized in Table 1.

(19) Gao, E.-Q.; Wang, Z.-M.; Yan, C.-H. *Chem. Commun.* **2003**, 1748−1749.

(20) (a) Dong, Y.-B.; Smith, M. D.; Layland, R. C.; zur Loye, H.-C. *Chem. Mater.* **2000**, *12*, 1156−1161. (b) Dong, Y.-B.; Smith, M. D.; zur Loye, H.-C. *Inorg. Chem.* **2000**, *39*, 4927−4935. (c) Gao, E. Q. *Acta Crystallogr.* **2005**, *C61*, O110−O111.

(21) Sheldrick, G. M. *SADABS, Empirical absorption correction program*, version 2.01; University of Göttingen: Göttingen, Germany, 1996.

(22) (a) Blessing, R. H. *Acta Crystallogr.* **1995**, *A51*, 33−38. (b) Blessing, R. H. *J. Appl. Crystallogr.* **1997**, *30*, 421−426.

(23) (a) Sheldrick, G. M. *SHELXTL*, version 5.1; Bruker Analytical X-ray Instruments Inc.: Madison, WI, 1998. (b) Sheldrick, G. M. *SHELXL-97*, PC version; University of Göttingen: Göttingen, Germany, 1997.

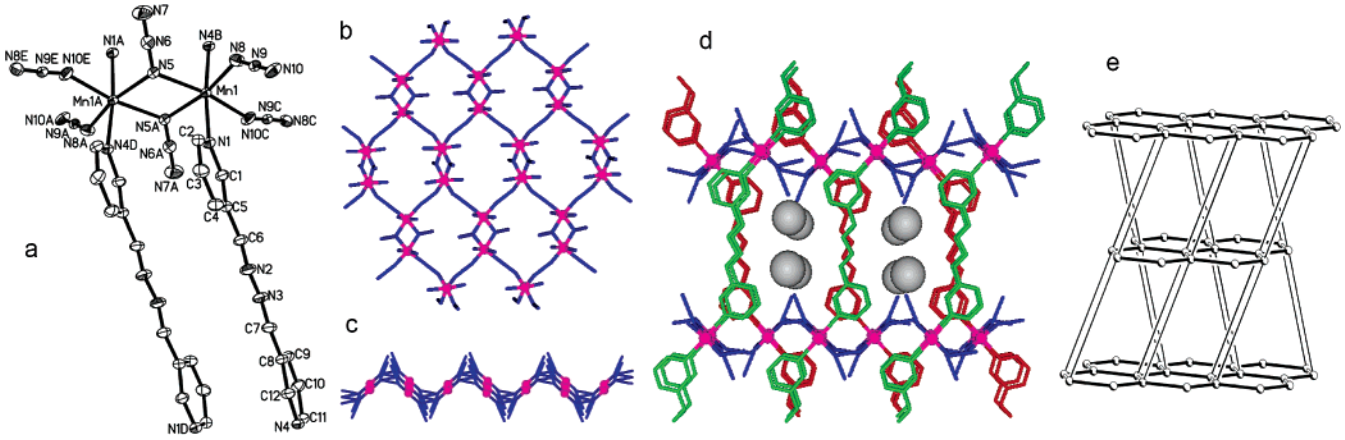

Figure 1. (a) View of the binuclear unit in complex **1** with the atom-labeling scheme. The thermal ellipsoids are drawn at 30% probability (A, $-x + {}^3/_2$, $-y + {}^1/_2$, $-z + 1$; B, $x + {}^1/_2$, $y - {}^1/_2$, z; C, $-x + {}^3/_2$, $y - {}^1/_2$, $-z + {}^3/_2$; D, $-x + 1$, $-y + 1$, $-z + 1$; E, x, $-y + 1$, $z - {}^1/_2$). (b) 2D azido-bridged Mn(II) layer. (c) Side view of the layer showing the undulated shape. (d) 3D network of **1** viewed down the *c* axis (gray balls: water molecules). (e) Illustration showing the five-connected net topology of **1**.

Table 2. Selected Bond Lengths and Angles for Complex **1**[a]

Mn1−N1	2.299(3)	Mn1−N4B	2.290(3)
Mn1−N5	2.255(3)	Mn1−N5A	2.232(3)
Mn1−N8	2.183(4)	Mn1−N10C	2.194(4)
N5−N6	1.205(5)	N8−N9	1.167(5)
N6−N7	1.148(5)	N9−N10	1.153(5)
N1−Mn1−N5	92.09(12)	N5−Mn1−N8	88.38(14)
N1−Mn1−N8	88.20(13)	N5−Mn1−N5A	77.34(14)
N1−Mn1−N5A	91.44(12)	N5−Mn1−N4B	93.11(12)
N1−Mn1−N4B	174.32(11)	N5−Mn1−N10C	169.57(15)
N1−Mn1−N10C	86.13(13)	N10C−Mn1−N5A	92.42(15)
N8−Mn1−N5A	165.69(14)	N10C−Mn1−N4B	89.16(13)
N8−Mn1−N4B	89.65(13)	N5A−Mn1−N4B	91.95(12)
N8−Mn1−N10C	101.83(16)	N9−N8−Mn1	137.0(3)
Mn1A−N5−Mn1	102.66(14)	N9−N10−Mn1D	152.7(3)
N6−N5−Mn1A	122.7(3)	N7−N6−N5	179.6(5)
N6−N5−Mn1	126.6(3)	N10−N9−N8	177.9(4)

[a] Symmetry codes: A, $-x + {}^3/_2$, $-y + {}^1/_2$, $-z + 1$; B, $x + {}^1/_2$, $y - {}^1/_2$, z; C, $-x + {}^3/_2$, $y - {}^1/_2$, $-z + {}^3/_2$; D, $-x + {}^3/_2$, $y + {}^1/_2$, $-z + {}^3/_2$.

Results and Discussion

Description of the Structures. (a) Complex 1. The complex **1** is a 3D coordination polymer built by the organic L^1 ligand interlinking 2D inorganic layers in which bis(μ-1,1-azido)-bridged dimanganese(II) units are joined by single EE azido bridges. Selected bond lengths and angles are listed in Table 2, and the structure is depicted in Figure 1.

Each Mn(II) ion in the complex assumes a trans pseudo-octahedral coordination geometry. The equatorial positions are occupied by four azido nitrogen atoms (N5, N8, N5A, and N10C), with the Mn−N distances ranging from 2.183(4) to 2.255(3) Å, and the axial positions are occupied by two pyridyl nitrogens (N1 and N4B) from different L^1 ligands, with the Mn−N distances [2.290(3) and 2.299(3) Å] being slightly elongated relative to those for azido ions. Two neighboring Mn(II) ions related by an inversion center are doubly linked by two EO azido bridges (N5 and N5A) to form a binuclear unit. In the resulting Mn_2N_2 planar ring, the Mn−N−Mn bridging angle is 102.7° and the Mn···Mn distance is 3.503 Å. These values lie in the typical range for double EO azido bridges.[6a] Through four azido bridges in the EE mode, each binuclear unit is connected to four neighboring identical motifs that are related to the original motif by 2_1 screw axes, generating a 2D manganese(II) azido layer (Figure 1b). The layers are parallel to the *bc* plane and exhibit a three-connected (6,3) topology, with Mn atoms as nodes and both double EO and single EE azido bridges as linkers. The Mn···Mn distance spanned by the EE bridge is 5.982 Å and the Mn−N−N−N−Mn torsion angle is 40.0°, suggesting a gauche conformation for the EE bridging moiety. The layer structure may also be described as single EE azido-bridged Mn(II) helical chains interlinked by the double EO azido bridges. The helical chains run around *2*-fold screw axes in the *b* direction, with the helical pitch being equal to the *b* dimension. The helicity leads to an systematic alternation of two different orientations of metal coordination spheres along the chain: the equatorial planes of the neighboring metal centers linked by single EE bridges are nearly perpendicular to each other with a dihedral angle of 85.6°. Closely related, the dihedral angle between neighboring Mn_2N_2 planar rings is 84.8°. These features are important in determining the 3D crystal structure and the spin-canted magnetic behaviors (see below). Because of the orientational alternation of the metal spheres and the gauche conformation of the EE bridging moiety, the inorganic layer is highly undulated (Figure 1c).

The 2D inorganic layers are pillared into a 3D inorganic−organic hybrid coordination network by the organic L^1 molecules, which connect Mn(II) ions from neighboring layers (Figure 1d). The pillar ligand adopts a nearly planar transoid conformation, and because of the off-axis coordination orientation of the ligand, the Mn···Mn distance (14.57 Å) spanned by the ligand is significantly longer than the interlayer separation (13.51 Å), defined as the distance between the mean Mn(II) planes of neighboring layers. The shortest interlayer Mn···Mn distance is 13.37 Å. As can be seen from Figure 1d, the undulated inorganic layers are stacked down the *a* direction in a concave-to-concave mode so that interlayer space can accommodate the long organic linkers comfortably by fitting the 3-pyridyl groups into the concave regions of the layers. The coordination orientation of the 3-pyridyl groups is complementary with the slanted orientation of the metal coordination spheres. The L^1 pillars

are stacked in an overlapping way to form 1D infinite arrays down the *c* direction, with weak $\pi-\pi$ interactions between pyridyl rings. The dihedral angles between the interacting aromatic rings are 4.8° for the two ligands bonded to the EO azido-bridged Mn ions and 10.1° for those bonded to the EE azido-bridged Mn ions. The separations between the rings are respectively 3.70 and 3.99 Å for centroid−centroid distances and 3.53 and 3.60 Å for interplane distances. The $\pi-\pi$-stacked arrays of the ligands divide the interlayer space into 1D channels down the *c* direction, in which disordered water molecules are included.

The 3D net of **1** arises from the offset stacking of 2D (6,3) nets and may be viewed as an irregular five-connected net with three different sets of linkers (the double EO bridges, the single EE azido bridges, and the L^1 pillars). A schematic illustration of the net is given in Figure 1e, and the Schläfli notation is $4^4 \cdot 6^6$, or $4^2 \cdot 4^2 \cdot 6 \cdot 6^2 \cdot 6^3$. The latter notation is used to differentiate the circuits that contain the same number of nodes but exhibit different geometries. Such a net is distinct from the known BN net ($4^6 \cdot 6 \cdot 6^3$), which is a simple prismatic stacking of planar (6,3) nets.[24]

Although the metal azido layers with alternate double EO and single EE azido bridges have been found in several 2D compounds,[7a,9,25] complex **1** is the first example of 3D coordination networks built by pillaring such layers.

(b) Complex 2. This complex is a 2D coordination polymer built by the organic L^2 ligand interlinking 1D manganese(II) azido chains of alternate double EO and double EE azido bridges. Perspective views of the 2D structure are shown in Figure 2, and selected bond lengths and angles are listed in Table 3.

Similar to that in **1**, the Mn(II) ion in **2** assumes a trans pseudo-octahedral coordination geometry, completed by four equatorial azido nitrogen atoms (N5, N8, N5B, and N10C) and two axial pyridyl nitrogens (N1 and N4A) with slightly elongated Mn−N distances (Table 3). However, adjacent Mn(II) ions in **2** are related by inversion centers and linked alternately by double EO and double EE azido bridges, affording 1D infinite chains along the *a* direction. In the double EO bridging moiety, the Mn···Mn distance is 3.459(3) Å and the Mn1−N5−Mn1B bridging angle is 102.6(1)°. These values lie in the typical range for Mn(II) ions with double EO azido bridges (100−105°).[6a] In the double EE bridging moiety, the Mn−N−N−N−Mn torsion angle (τ) is 30.4(3)° and the dihedral angle (δ) between the N8−Mn1−N10C plane and the plane defined by the two EE azido ions is 18.2(2)°, indicating a slight chair conformation for the Mn−$(N_3)_2$−Mn ring. Both τ and δ in **2** lie in the ranges (19−64° for τ and 8.9−35° for δ) reported previously for Mn(II) chains with alternating EE and EO bridges.[6a] The Mn···Mn distance spanned by the EE bridge is 5.188(3) Å.

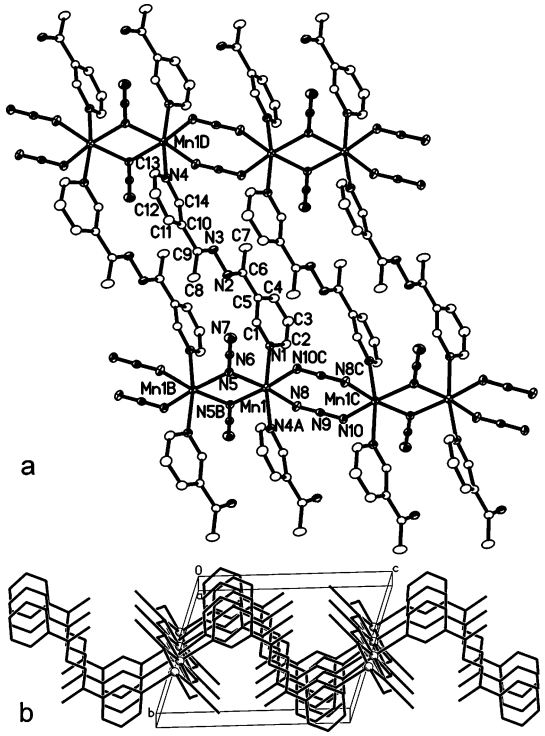

Figure 2. Top (a) and side views (b) of the 2D network in complex **2** (A, $x-1, y, z-1$; B, $-x+1, -y+1, -z$; C, $-x, -y+1, -z$; D, $x+1, y, z+1$).

Table 3. Selected Bond Lengths and Angles for Complex **2**[a]

Mn1−N1	2.319(2)	Mn1−N4A	2.324(2)
Mn1−N5	2.221(3)	Mn1−N5B	2.211(2)
Mn1−N8	2.208(3)	Mn1−N10C	2.233(3)
N5−N6	1.210(3)	N8−N9	1.181(4)
N6−N7	1.146(3)	N9−N10	1.168(3)
N1−Mn1−N5	92.82(9)	N5−Mn1−N8	170.39(9)
N1−Mn1−N8	89.31(9)	N5−Mn1−N4A	91.32(9)
N1−Mn1−N4A	169.08(9)	N5−Mn1−N5B	77.39(10)
N1−Mn1−N5B	97.58(9)	N5−Mn1−N10C	91.19(10)
N1−Mn1−N10C	86.23(9)	N5B−Mn1−N4A	93.18(9)
N8−Mn1−N4A	88.28(9)	N10C−Mn1−N4A	83.59(9)
N8−Mn1−N5B	93.05(10)	N5B−Mn1−N10C	168.09(10)
N8−Mn1−N10C	98.29(11)	Mn1−N5−Mn1B	102.61(10)
N6−N5−Mn1B	130.4(2)	N9−N8−Mn1	125.5(2)
N6−N5−Mn1	126.1(2)	N9−N10−Mn1C	129.1(2)
N7−N6−N5	179.1(3)	N10−N9−N8	177.7(3)

[a] Symmetry codes: A, $x-1, y, z-1$; B, $-x+1, -y+1, -z$; C, $-x, -y+1, -z$.

The inorganic manganese(II) azido chains are interlinked into 2D inorganic−organic hybrid layers by the organic L^2 linkers (Figure 2). The L^2 ligand adopts a slightly twisted trans conformation with respect to the central N−N bond, with the dihedral angle between the two pyridyl rings being 15.9°. The Mn···Mn distance spanned by L^2 is 12.69 Å, significantly shorter than that in **1**. This is mainly due to the different conformations of the pyridylimine groups: For L^1 in **1**, the pyridylimine groups are trans in that the pyridyl donor atom and the imine nitrogen atom are at different sides of the $C_{imine}-C_{py}$ bond, while for L^2 in **2**, the pyridylimine groups are cis in that the pyridyl donor atom and the imine nitrogen atom are at the same side of the $C_{imine}-C_{py}$ bond. The layer is highly undulated (Figure 2b) because of the slanted disposition of the L^1 ligand with respect to the

(24) O'Keeffe, M.; Eddaoudi, M.; Li, H.; Reineke, T.; Yaghi, O. M. *J. Solid State Chem.* **2000**, *152*, 3−20.
(25) (a) Escuer, A.; Vicente, R.; Goher, M. A. S.; Mautner, F. A. *Inorg. Chem.* **1997**, *36*, 3440−3446. (b) Escuer, A.; Cano, J.; Goher, M. A. S.; Journaux, Y.; Lloret, F.; Mautner, F. A.; Vicente, R. *Inorg. Chem.* **2000**, *39*, 4688−4698.

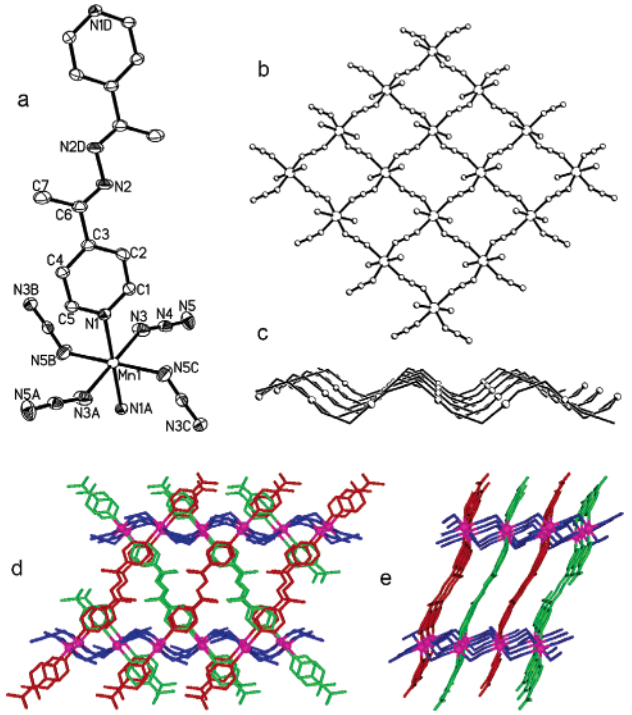

Figure 3. (a) View of the building block in complex **3** with the atom-labeling scheme. The thermal ellipsoids are drawn at 30% probability (A, $-x+1, -y+1, -z$; B, $-x+1, y-{}^1/_2, -z+{}^1/_2$; C, $x, -y+{}^3/_2, z-{}^1/_2$; D, $-x+2, -y, -z+1$). (b) 2D azido-bridged Mn(II) layer. (c) Side view showing the undulated shape of the layer. (d and e) 3D network of **3** viewed down the *c* and *b* axes, respectively.

M···M line. The slanted disposition is dictated by the specific off-axis coordination orientation of the terminal 3-pyridyl rings [the angle between the M−N bond and the N(donor)···N(donor) line is about 120°]. The layers are stacked in parallel, and the shortest interlayer Mn···Mn distance is 8.62 Å.

Although a relatively large family of 1D manganese(II) azido chains with alternate double EO and double EE bridges have been reported,[6a] complex **2** represents the first example of 2D inorganic−organic hybrid networks built from these kinds of chains. A related 2D network built from alternating manganese(II) azido chains was reported very recently in which azido bridges alternate in the double EE, double EE, and double EE sequence and the organic linker is 4,4′-bipyridylethene.[16a]

(c) Complex 3. This complex is a 3D coordination polymer built by the organic L^3 ligand interlinking 2D inorganic layers in which Mn(II) ions are joined by single EE azido bridges. Some views illustrating the structure are shown in Figure 3, and selected bond lengths and angles are listed in Table 4.

Again, the metal atom in **3** is ligated by four equatorial azido ions and two axial pyridyl nitrogens from the organic ligands (Figure 3a), affording a trans octahedral environment with slight axial elongation (Table 3). However, here all of the azido ions are equivalent (related by inversion centers or 2-fold screw axes) and adopt the single EE bridging mode. Thus, each Mn(II) ion, which resides at a inversion center, is connected to four neighbors via four single EE azido bridges, yielding neutral 2D (4,4) quadratic manganese(II)

Table 4. Selected Bond Lengths and Angles for Complex **3**[a]

Mn1−N1	2.281(2)	N3−N4	1.158(4)
Mn1−N3	2.191(3)	N4−N5	1.165(4)
Mn1−N5B	2.215(3)	N2−N2D	1.406(5)
N1−Mn1−N1A	180.0	N3−Mn1−N3A	180.0
N1−Mn1−N3	87.75(10)	N3−Mn1−N5B	92.32(15)
N1−Mn1−N3A	92.25(10)	N3−Mn1−N5C	87.68(15)
N1−Mn1−N5B	89.97(10)	N5B−Mn1−N5C	180.0
N1−Mn1−N5C	90.03(10)	N3−N4−N5	175.2(4)
N4−N3−Mn1	146.1(3)	N4−N5−Mn1E	128.6(3)

[a] Symmetry codes: A, $-x+1, -y+1, -z$; B, $-x+1, y-{}^1/_2, -z+{}^1/_2$; C, $x, -y+{}^3/_2, z-{}^1/_2$; D, $-x+2, -y, -z+1$; E, $-x+1, y+{}^1/_2, -z+{}^1/_2$.

azido layers parallel to the *bc* plane (Figure 3b). The Mn−N−N−N−Mn torsion angle and the Mn- - -Mn distance spanned by the bridge are 94.6(3)° and 5.918 Å, respectively. Adjacent Mn atoms are related by 2-fold screw axes, which leads to an systematic alternation of slanted coordination polyhedrons throughout the layer: the equatorial plane of each Mn(II) ion is slanted relative to the layer plane with a dihedral angle of 40.9°, and the dihedral angle between neighboring MnN_4 equatorial planes is 81.6°. The systematic alternation in coordination orientation leads to an undulated shape for the manganese(II) azido layer (Figure 3c).

The inorganic layers are pillared by the organic L^3 spacers to generate a hybrid 3D architecture (Figure 3d,e). The pillar ligands reside on inversion centers, adopt a planar trans conformation, and separate Mn(II) ions by 15.62 Å. This distance is longer than that separated by L^1 in **1** because of the different substitution positions on the pyridyl rings. To adapt to the slanted orientations of the coordination spheres in the layers, the L^1 linkers are also slanted markedly, with two different orientations alternating down the *c* direction. As a result, the interlayer separation (12.13 Å) and the shortest interlayer Mn···Mn distance (12.56 Å) are much shorter than the Mn···Mn distance separated by the ligand. The former two distances are also much shorter than those in **1**.

Only five manganese(II) azido compounds containing single EE azido-bridged (4,4) layers have been reported elsewhere,[7c,10,13,26] of which two are 3D pillared-layer networks with pyrimidine (pym)[10] and pyrazine-*N*,*N*′-dioxide (pzdo)[13] as pillars. The undulated 2D layer in **3** is very similar to those observed in the 2D compounds $[Mn(4\text{-acpy})_2(N_3)_2]_n$[26a] and $[Mn(minc)_2(N_3)_2]_n$[26b] (4-acpy = 4-acetylpyridine; minc = methyl isonicotinate) and the 3D compound $[Mn(pym)(N_3)_2]_n$, where the dihedral angles between neighboring MnN_4 equatorial planes are in the range of 70.9−84.9°. It seems that the undulated shape of the layers is induced (or templated) by the coordination of the pyridyl or pyrimidine rings, which fit well with the concaves of the layers. In the other 3D compound $[Mn(pzdo)(N_3)_2]_n$, where the donors are the oxygen atoms of the *N*-oxide group, the layer is only slightly undulated, which is related to a much smaller dihedral angle (47.0°) between neighboring MnN_4

(26) (a) Escuer, A.; Vicente, R.; Goher, M. A. S.; Mautner, F. A. *Inorg. Chem.* **1995**, *34*, 5707−5708. (b) Escuer, A.; Vicente, R.; Goher, M. A. S.; Mautner, F. A. *J. Chem. Soc., Dalton Trans.* **1997**, 4431−4434.

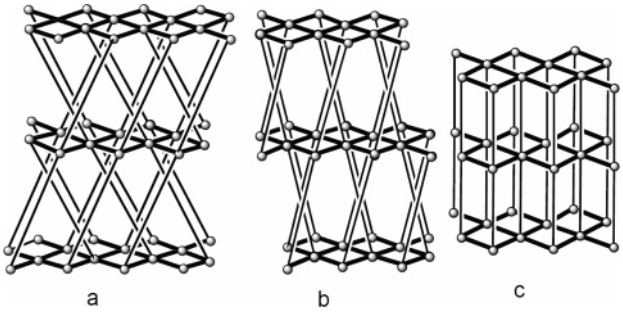

Figure 4. Illustrations of some 3D nets built by pillaring (4,4) layers.

Chart 2. Schematic Illustrations of the Connection Patterns between the Undulated Layers[a]

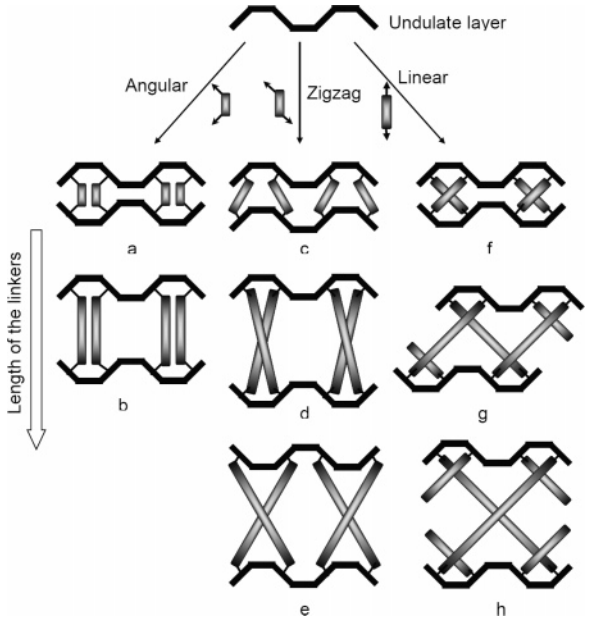

[a] The 3D nets correspond to Figure 4c for parts a−c, Figure 4b for parts d−f, and Figure 4a for part g.

equatorial planes. In the third 2D compound $[Mn(DEAN)_2(N_3)_2]_n$ (DENA = *N*,*N*′-diethylnicotinamide),[7c] the layer is very flat, with the corresponding dihedral angle being only 5.6°, perhaps because of the steric effect of the large dimethylcarboxamide group on the 3 position of the pyridyl rings.

Because of the different patterns of the interlayer connection, the 3D net (Figure 4a) of **3** is distinct from those (Figure 4c) of the two previous 3D compounds,[10,13] although they are all irregular six-connected nets with two different kinds of linkers (the single EE azido bridges and the pillars). The Schläfli notations of the nets are $4^4 \cdot 6^2 \cdot 6^8 \cdot 8$ for **3** but $4^4 \cdot 4^8 \cdot 6 \cdot 6^2$ for the previous compounds. The latter net is an irregular variation of the simple primitive cubic net ($4^{12} \cdot 6^3$).[24] The interlayer packing and the 3D net of these complexes seem to be the consequence of the interplay between the slanted metal coordination orientation in the undulated layers and the length and geometry of the interlayer linkers (Chart 2). The angular coordination geometry of the pym linker is complementary with the orientations of the metal spheres in the layers, and hence the ligand can join two differently orientated metal spheres from different layers. This requires that neighboring layers be stacked in a concave-to-concave fashion (Chart 2a). The zigzag coordination conformation of the pzdo ligand makes it join two metal spheres of the same orientation, and the specific length of the ligand makes the layers stack in a concave-to-convex fashion. The features of pym and pzdo compensate for the different orientations of the metal spheres in the layers, leading to the simple quasi-cubic nets (Figure 4c). The nearest interlayer Mn···Mn distances in these two compounds are 6.15 and 6.42 Å, respectively, which are much shorter than that in **3**. In **3**, the quasi-linear L^3 linkers have to slant markedly in two different orientations to be in accord with the slanted metal spheres, and the specific length of the linkers dictates a concave-to-convex interlayer stacking fashion (Chart 2g) and a different 3D net (Figure 4a). To illustrate the influence of the length and geometry of the linkers on the interlayer packing and the 3D net, some other possibilities are also given in Chart 2. While a length change of the angular linkers leads to a change in the interlayer distance without changes in the interlayer stacking fashion and net topology (Chart 2a,b), the length change of the zigzag or linear linkers not only leads to the change in the interlayer distance but also may cause changes in the interlayer stacking fashion and/or net topology. For example, elongating the zigzag linkers to specific lengths would lead to the interlayer connection patterns illustrated in Chart 2d,e, and the resulting structures would exhibit the new net topology shown in Figure 4b (Schläfli notation $4^4 \cdot 4^4 \cdot 6^2 \cdot 6^4 \cdot 8$). The same net topology is also expected with very short linear linkers (Chart 2f), and elongating the linear linkers to specific lengths may result in another new 3D net, for which the interlayer connection pattern is illustrated in Chart 2h. These demonstrate the potentials of tuning the 3D structure through organic linkers.

The 3D net of **1** is closely related: taking the double EO bridged $[Mn_2(N_3)_2]$ motifs in **1** as nodes that correspond to the single Mn(II) ions in **3**, the manganese(II) azido layer in **1** becomes a quadratic (4,4) network with single EE azido bridges as linkers, and then the five-connected net illustrated in Figure 1e is reduced to the six-connected net illustrated in Figure 4b and Chart 2d.

(d) Complex 4. This complex is a 2D coordination polymer in which single EE azido-bridged manganese(II) chains are interlinked by the L^4 ligand. The structure is shown in Figure 5, and selected bond lengths and angles are listed in Table 5.

There are two independent sets of Mn(II) ions in **4**, and the coordination environments around them are different from each other and from those in the previous complexes, although all are pseudo-octahedral with comparable bond lengths. The Mn1 ion, which resides on a 2-fold axis along the *b* direction, is ligated by two terminal azido ions (N5 and N5A) in cis positions, two EE bridging azido ions (N8 and N8A) in trans positions, and two pyridyl nitrogens (N1 and N1A) from the organic ligands in cis positions. Differently, the Mn2 ion is placed at an inversion center with a trans-coordination sphere, which is completed by two EE bridging azido ions (N10 and N10B), two methanol molecules (O1 and O1B), and two pyridyl nitrogens (N4C and N4D). The EE azido bridges join the Mn1 and Mn2 ions

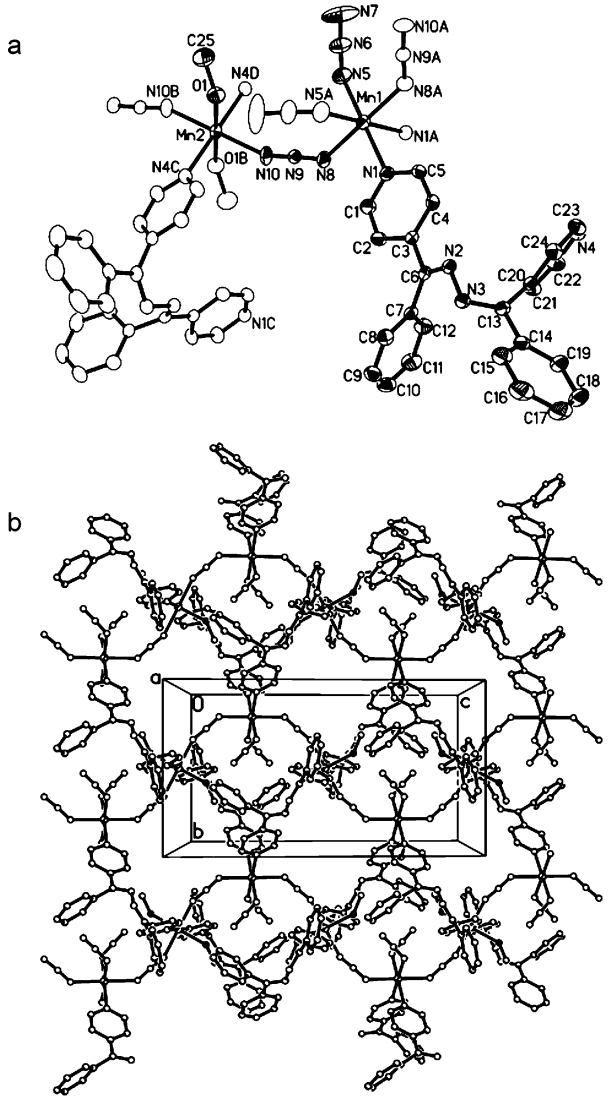

Figure 5. Structure of **4**: (a) a perspective view showing the coordination environments and the atom-labeling scheme. Thermal ellipsoids are drawn at 30% probability, and the symmetry-generated atoms are drawn as open ellipsoids to highlight the asymmetric unit. (b) 2D layer.

Table 5. Selected Bond Lengths and Angles for Complex **4**[a]

Mn1−N1	2.295(3)	Mn2−O1	2.199(3)
Mn1−N5	2.183(4)	Mn2−N10	2.170(4)
Mn1−N8	2.240(4)	Mn2−N4C	2.299(3)
N5−N6	1.138(5)	N8−N9	1.164(4)
N6−N7	1.124(6)	N9−N10	1.165(4)
N1−Mn1−N5	179.45(15)	N10−Mn2−N10B	180.0
N1−Mn1−N5A	89.79(14)	N10−Mn2−O1	89.55(15)
N1−Mn1−N8A	89.63(13)	N10−Mn2−O1B	90.45(15)
N1−Mn1−N8	90.31(12)	N10−Mn2−N4D	88.13(13)
N1−Mn1−N1A	89.80(16)	N10−Mn2−N4C	91.87(13)
N5−Mn1−N5A	90.6(2)	O1−Mn2−O1B	180.0
N5−Mn1−N8A	90.75(15)	O1−Mn2−N4D	91.25(12)
N5−Mn1−N8	89.31(15)	O1−Mn2−N4C	88.75(12)
N8−Mn1−N8A	179.92(19)	N4C−Mn2−N4D	180.0
N6−N5−Mn1	126.3(3)	C25−O1−Mn2	129.4(4)
N7−N6−N5	175.9(7)	N8−N9−N10	176.3(4)
N9−N8−Mn1	136.0(3)	N9−N10−Mn2	155.9(3)

[a] Symmetry codes: A, $-x+1, y, -z+1/2$; B, $-x+1, -y, -z$; C, $x, -y+1, z-1/2$; D, $-x+1, y-1, -z+1/2$.

alternately to generate a 1D singly bridged sinusoidal chain along the *c* direction (Figure 5b). The Mn1···Mn2 distance separated by the azido bridge is 6.03 Å, and the Mn1−N−N−N−Mn2 torsion angle is only 0.7°. Along the chain, neighboring coordination octahedra are markedly slanted with respect to each other, as indicated by the angle (115.5°) between the N8−Mn1−N8A line and the N10−Mn2−N10B line or the dihedral angle (64.4°) between the neighboring Mn1 and Mn2 equatorial planes (assuming the azido bridges as the axial ligands).

The 1D chains are interlinked by the organic L^4 ligand to produce 2D hybrid layers parallel to the *bc* crystallographic plane. While the corresponding organic ligands in **1**−**3** adopt quasi-planar conformations, L^4 in **4** distorts severely from planarity, and none of the aromatic rings are coplanar with one another. The dihedral angle between the two pyridyl rings is 62.7°, and the torsion angle for the central C═N−N═C linkage is 63.2°. The Mn1···Mn2 distance spanned by the ligand is 8.91 Å, which is much shorter than those in the previous complexes due to the twist of L^4 in **4**. The layers are stacked down the *c* direction with deep interdigitation between neighboring layers. The shortest interlayer metal-to-metal distance is 12.76 Å between Mn1 and Mn2 ($x-1/2, y+1/2, z$).

Although single EE azido-bridged M(II) chains have been found in many Ni(II) and Cu(II) species[27,28] and a few Mn(III) species,[29] it should be noticed that only two Mn(II) analogues have been reported. One is a 1D chain compound with single EE azido bridges in trans positions of the metal centers, where the trans coordination of the azido ions was believed to be forced by preformed planar Mn(II) macrocycle units.[30] The other one, reported very recently, is a 1D compound with single EE azido bridges in cis positions.[16a] Complex **4** represents the first 2D compound in which single EE azido-bridged Mn(II) chains are interlinked by an organic ligand. It is interesting to note that the single azido bridges are in trans positions, although no macrocyclic ligand is involved.

Magnetic Properties. (a) Complex 1. The temperature dependences of magnetic susceptibility (χ_M) and its product with temperature ($\chi_M T$) for compound **1** at an applied field of 5 kG are shown in Figure 6. The $\chi_M T$ value per Mn(II) at

(27) (a) Maji, T. K.; Mukherjee, P. S.; Mostafa, G.; Mallah, T.; Cano-Boquera, J.; Chaudhuri, N. R. *Chem. Commun.* **2001**, 1012−1013. (b) Woodard, B.; Willett, R. D.; Haddad, S.; Twamley, B.; Gomez-Garcia, C. J.; Coronado, E. *Inorg. Chem.* **2004**, *43*, 1822−1824. (c) Mukherjee, P. S.; Maji, T. P.; Escuer, A.; Vicente, R.; Ribas, J.; Rosair, G.; Mautner, F. A.; Chaudhuri, N. R. *Eur. J. Inorg. Chem.* **2002**, 943−949.

(28) (a) Mukherjee, P. S.; Dalai, S.; Zangrando, E.; Lloret, F.; Chaudhuri, N. R. *Chem. Commun.* **2001**, 1444−1445. (b) Monfort, M.; Resino, I.; El Fallah, M. S.; Ribas, J.; Solans, X.; Font-Bardia, M.; Stoeckli-Evans, H. *Chem.—Eur. J.* **2001**, *7*, 280−287. (c) Hong, C. S.; Do, Y. *Angew. Chem., Int. Ed.* **1999**, *38*, 193−195. (d) Escuer, A.; Harding, C. J.; Dussart, Y.; Nelson, J.; McKee, V.; Vicente, R. *J. Chem. Soc., Dalton Trans.* **1999**, 223−227. (e) Escuer, A.; Vicente, R.; Ribas, J.; El Fallah, M. S.; Solans, X.; Font-Bardía, M. *Inorg. Chem.* **1994**, *33*, 1842−1847. (f) Ribas, J.; Monfort, M.; Ghosh, B. K.; Cortés, R.; Solans, X.; Font-Bardía, M. *Inorg. Chem.* **1996**, *35*, 864−868.

(29) (a) Reddy, K. R.; Rajasekharan, M. V.; Tuchagues, J. P. *Inorg. Chem.* **1998**, *37*, 5978−5982. (b) Li, H.; Zhong, Z. J.; Duan, C. Y.; You, X. Z.; Mak, T. C. W.; Wu, B. *Inorg. Chim. Acta* **1998**, *271*, 99−104. (c) Panja, A.; Shaikh, N.; Vojtíxf0ek, P.; Gao, S.; Banerjee, P. *New J. Chem.* **2002**, *26*, 1025−1028.

(30) Sra, A. K.; Sutter, J. P.; Guionneau, P.; Chasseau, D.; Yakhmi, J. V.; Kahn, O. *Inorg. Chim. Acta* **2000**, *300*−*302*, 778−782.

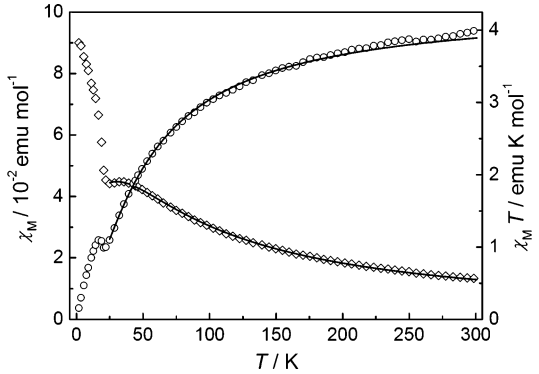

Figure 6. Temperature dependences of χ_M and $\chi_M T$ for **1**. The solid lines represent the best fit of the experimental data to eqs 1 and 2.

300 K is ca. 4.0 emu K mol^{-1}, lower than the spin-only value (4.38 emu K mol^{-1}) expected for a magnetically isolated high-spin Mn(II) ion with $g = 2.00$. As the sample is cooled from room temperature, χ_M first increases smoothly to reach a rounded maximum of 0.045 emu mol^{-1} at about 33 K, then decreases slightly to 0.044 emu mol^{-1} at 25 K, and finally increases rapidly to 0.090 emu mol^{-1} at 1.8 K. On the other hand, $\chi_M T$ first decreases upon cooling to a minimum of 0.98 emu K mol^{-1} at 21 K, and then after a slight increase to a maximum of 1.1 emu K mol^{-1} at 17 K, it decreases again upon further cooling to 1.8 K.

The magnetic behaviors of **1** above 25 K are typical of 1D or 2D Mn(II) complexes with dominant AF interactions. It has been demonstrated by many Mn(II) complexes that the interaction between azido-bridged Mn(II) ions is AF for the EE bridging mode but F for the EO mode. Therefore, we can assume that compound **1** exhibits F and AF interactions through double EO and single EE azido bridges, respectively. To evaluate the magnetic interactions, we applied an approximate approach that has been used for similar 2D layers.[7a,25c] This approach treated the 2D layer as EE azido-bridged AF chains interacting ferromagnetically through the double EO azido bridges. The AF interaction (*J*) through the EE azido bridge can be accounted for by the conversional equation derived by Fisher for a uniform chain of classical spins based on the Hamiltonian $\mathbf{H} = -J\sum \mathbf{S}_i\mathbf{S}_{i+1}$:[31a]

$$\chi_{chain} = [Ng^2\beta^2S(S+1)/(3kT)][(1+u)/(1-u)] \quad (1)$$

where u is the well-known Langevin function defined as $u = \coth[JS(S+1)/kT] - kT/[JS(S+1)]$ with $S = {}^5/_2$. The interaction through the interchain EO azido bridges may be reduced to the interchain interaction (zJ') using the molecular field approximation:[31b]

$$\chi_M = \chi_{chain}/[1 - (zJ'/Ng^2\beta^2)\chi_{chain}] \quad (2)$$

With g fixed at 2.00, the least-squares fit of the experimental data above 25 K to the above expressions led to $J = -5.1$ cm^{-1} and $zJ' = 1.9$ cm^{-1}. We have omitted the very weak, if any, interlayer interaction through the organic spacers because of the large metal-to-metal separation between layers. The above values are in good agreement with those (-4.5 to -5.4 cm^{-1} for J and 1.1−3.1 cm^{-1} for zJ') reported previously for 2D Mn(II) complexes with the same azido bridging network[7a,25c] and confirm that the interactions mediated via the single EE and the double EO bridges are AF and F, respectively.

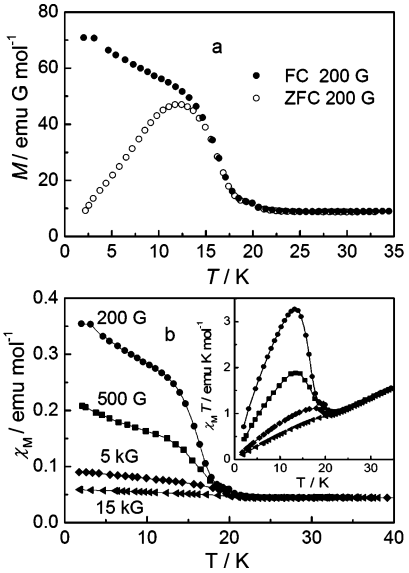

Figure 7. FC and ZFC magnetization plots at 200 G (a) and FC magnetizations in the forms of χ_M and $\chi_M T$ (inset) vs T plots at different fields (b) for **1**.

Although the AF/F intralayer interactions tend to align the Mn(II) spins within the layer in a compensated way to give a zero residual moment, the low-temperature magnetic behaviors (the abrupt rises in both χ_M and $\chi_M T$) of **1** suggest the existence of uncompensated residual spin moments and the occurrence of long-range weak F ordering. The weak ferromagnetism may be attributed to spin canting: the antiferromagnetically coupled local spins within the layers are not perfectly antiparallel but canted to each other, resulting in uncompensated residual spins. The correlation between the residual spins may lead to long-range ordering. For **1**, the rise in $\chi_M T$ below 21 K indicates a F-like correlation. To confirm the weak ferromagnetism, FC (field-cooled) and ZFC (zero-field-cooled) magnetization measurements were performed at 200 G (Figure 7a). It is clear that **1** exhibits weak spontaneous magnetization due to the onset of long-range ordering of the canted spins, and the divergence of the ZFC and FC data below $T_c = 16$ K indicates irreversibility arising from the formation of an ordered magnetic state. For a weak ferromagnet due to spin canting, the magnetic behavior should be quite field-dependent. Thus, FC magnetizations were measured at different applied fields (Figure 7b). As can be seen, the rises of the χ_M and $\chi_M T$ values at low temperature become less pronounced at higher fields, and the $\chi_M T$ curve shows no rise anymore at the field of 15 kG, although a change in the curvature is still perceptible.

Further experimental evidences for the spin-canted weak ferromagnetism in **1** come from field-dependent isothermal magnetization measurements at 1.8 K (Figure 8). In the high-

(31) (a) Fisher, M. E. *Am. J. Phys.* **1964**, *32*, 343−348. (b) O'Connor, C. J. *Prog. Inorg. Chem.* **1982**, *29*, 203−283.

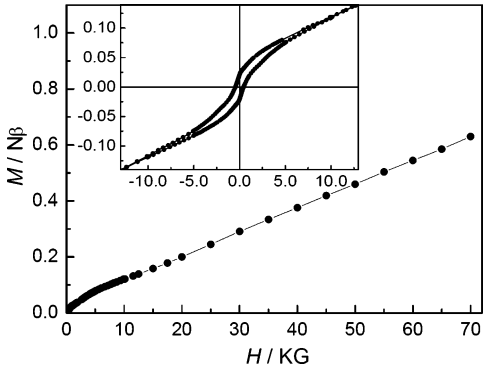

Figure 8. Field dependence of magnetization of **1** at 1.8 K. The hysteresis loop is shown as an inset.

field region (H > 20 kG), the magnetization increases slowly and linearly with the field, and the magnetization value (0.63 Nβ) achieved at the highest field measured (70 kG) is far below the saturation value (5 Nβ) expected for Mn(II) species. These features support the overall AF interaction in **1**. However, the magnetization curve of **1** is different from that of a 2D Heisenberg antiferromagnet in that the initial increase of magnetization at low fields is relatively rapid and nonlinear. This feature is consistent with spin canting in an AF system. A hysteresis loop was observed at 1.8 K with a remnant magnetization (M_r) of 0.020 Nβ and a coercive field (H_c) of 450 G (Figure 8, inset), confirming the weak F ordering. Extrapolating the reversible linear part of the hysteresis curve to zero field gives a magnetization value of 0.044 Nβ. Assuming this to be the F saturation magnetization due to spin canting (M_F, i.e., the maximum contribution of spin canting to the total magnetization), the spin-canting angle α is estimated[32] to be about 0.5°, according to the equation $\tan \alpha = M_F/M_S$, where M_S is the saturation magnetization (5 Nβ) expected for a Mn(II) system.

The spin-canting behavior of **1** is consistent with the structural observation that the compound contains single EE azido-bridged helical Mn(II) chains, in which the coordination polyhedra are alternately slanted with respect to each other. It is well-known that spin canting may arise from single-ion magnetic anisotropy and/or antisymmetric exchange (Dzyaloshinsky−Moriya interaction).[33,34] Both mechanisms require that no inversion center is present between the interacting spin centers. For compound **1**, although the double EO azido bridging moiety is centrosymmetric, there are no inversion centers within the single EE azido-bridged chain. It is expected that spin canting can occur throughout the chain. The observed weak ferromagnetism is due to the F long-range ordering of the spin-canted chains. Considering the isotropic character of the Mn(II) ion, it was often suggested that the Dzyaloshinsky−Moriya interaction is the main source of spin canting in Mn(II) compounds.[11a,34] However, magnetic anisotropy due to zero-field splitting may dominate in cases where the coordination octahedra suffer a significant distortion.[6c,34a] In **1**, the longest Mn−N distance is 0.116(4) Å longer than the shortest, and the maximum difference in the cis N−Mn−N angles is 24.5(2)°. This may suggest that the spin canting has a significant contribution from the magnetic anisotropy due to the zero-field splitting.

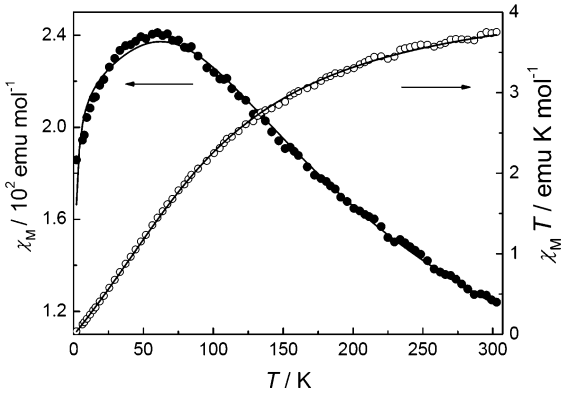

Figure 9. Temperature dependences of χ_M and $\chi_M T$ for **2**. The solid lines represent the best fit of the experimental data to eq 3.

Despite the 3D structure, the spin-canting behavior of compound **1** is similar to those for most 2D Mn azido compounds with the same single EE−double EO bridging network.[7a,9,25] As we have analyzed recently,[7a] only the compound $[Mn(dmbpy)(N_3)_2]_n$ (dmbpy = 4,4′-dimethyl-2,2′-bipyridine)[25c] does not exhibit spin canting, consistent with the fact that the single EE azido bridges in the compound are crystallographically centrosymmetric. All other 2D compounds contain noncentrosymmetric single EE azido bridges and exhibit spin-canting behaviors. [7a]

(b) Complex 2. The temperature dependence of magnetic susceptibility (χ_M) for compound **2** is shown in Figure 9. The $\chi_M T$ value per Mn(II) at 300 K is ca. 3.74 emu K mol^{-1}, which is lower than the spin-only value (4.38 emu K mol^{-1}) for a magnetically isolated Mn(II) system. As the temperature is decreased, the $\chi_M T$ value decreases monotonically, whereas χ_M increases to a rounded maximum of 0.024 emu mol^{-1} at about 58 K and then decreases upon further cooling to 2 K. These features suggest that the dominant magnetic exchange between Mn(II) ions is AF in nature.

According to structural data, the 2D compound **2** consists of azido-bridged alternate Mn(II) chains cross-linked by long organic spacers. The thermal variation of the magnetic properties shown in Figure 9 are very similar to those of previously reported 1D Mn(II) chain compounds with alternate double EO and double EE azido bridges, which mediate F and AF interactions, respectively. The intrachain magnetic interactions through the azido bridges can be evaluated using the expression proposed by Cortés et al. for alternate chains of classical spins based on the Hamiltonian $\mathbf{H} = -J_1\sum \mathbf{S}_{2i}\mathbf{S}_{2i+1} - J_2\sum \mathbf{S}_{2i+1}\mathbf{S}_{2i+2}$:[36]

$$\chi_M = [Ng^2\beta^2S(S+1)/3k(T-\theta)][(1+u_1+u_2+u_1u_2)/(1-u_1u_2)] \quad (3)$$

(32) Bellitto, A.; Federici, F.; Colapietro, M.; Portalone, G.; Caschera, D. *Inorg. Chem.* **2002**, *41*, 709−714.
(33) (a) Dzyaloshinsky, I. *Phys. Chem. Solids* **1958**, *4*, 241−255. (b) Moriya, T. *Phys. Rev.* **1960**, *120*, 91−98.
(34) (a) Carlin, R. L. *Magnetochemistry*; Springer-Verlag: Berlin, 1986; pp 148−154. (b) Batten, S. R.; Jensen, P.; Kepert, C. J.; Kurmoo, M.; Moubaraki, B.; Murray, K. S.; Price, D. J. *J. Chem. Soc., Dalton Trans.* **1999**, 2987−2997. (c) Carling, S. G.; Day, P.; Visser, D.; Kremer, R. K. *J. Solid State Chem.* **1993**, *106*, 111−119.

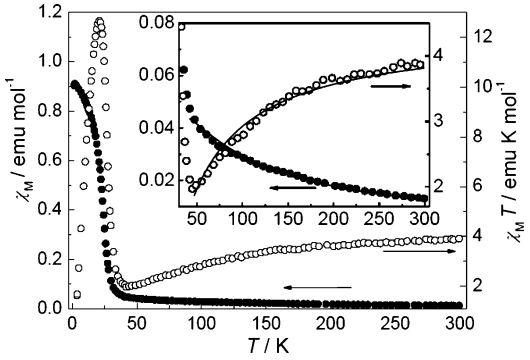

Figure 10. Temperature dependences of χ_M and $\chi_M T$ for **3**. The inset shows the high-temperature data and the best fit (solid lines) to the Lines expression (eq 4).

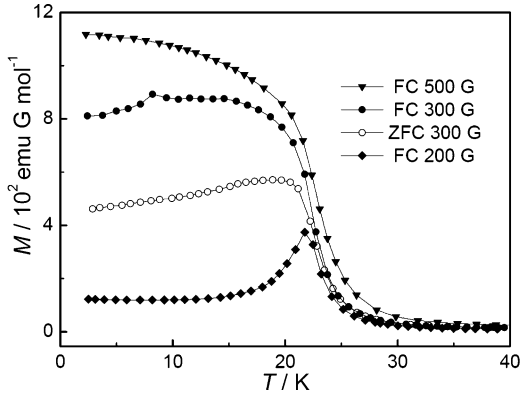

Figure 11. FC and ZFC magnetization plots at different fields for **3**.

where u_i is the Langevin function defined as $u_i = \coth[J_iS(S + 1)/kT] - kT/[J_iS(S + 1)]$ ($i = 1$ and 2) with $S = {}^5/_2$, J_1 and J_2 are the exchange constants for the EO and EE superexchange pathways, respectively, and θ was used to correct the possible secondary effects such as interchain AF interactions and/or zero-field splitting of the Mn(II) ion. With the g parameter fixed at 2.0, the best fit of the experimental data led to $J_1 = 7.8$ cm^{-1}, $J_2 = -15.9$ cm^{-1}, and $\theta = -0.66$ K. The J_1 and J_2 parameters confirm alternating F and AF interactions, with the latter one dominating. We have recently collected and compared the magnetostructural data for the known Mn(II) chains with double EO and/or double EE bridges,[6a] and the general trends are that the F interaction via a double EO bridge increases as the Mn−N−Mn bridging angle is increased and that the AF interaction via a double EE bridge decreases as the δ angle [the dihedral angle between the N(azido)−M−N(azido) plane and the plane defined by the two azido bridges] is increased. With Mn−N−Mn = 102.6(1)° and δ = 18.2(2)°, compound **2** follows the trends very well.

(c) Complex 3. The temperature-dependent magnetic behaviors of compound **3** under 2 kG in the 2−300 K range were shown in the forms of χ_M and $\chi_M T$ vs T plots in Figure 10. The $\chi_M T$ value per Mn(II) at 300 K is ca. 3.91 emu K mol^{-1}, lower than the value expected for a magnetically isolated Mn(II) ion. The susceptibility increases slowly as the sample is cooled from room temperature to 42 K, but it rises abruptly upon further cooling and tends to saturate at lower temperatures. On the other hand, $\chi_M T$ first decreases smoothly upon cooling to a rounded minimum of 1.97 emu K mol^{-1} at about 40 K, then rises rapidly to a sharp maximum of 12.7 emu K mol^{-1} at about 19 K, and finally drops rapidly upon further cooling to 1.8 K. The $\chi_M T$ maximum is well over the expected value for a Mn(II) ion. The magnetic behaviors above 42 K clearly indicate that the interaction between Mn(II) is AF, as expected for the azido bridges in the EE mode. The abrupt rises in χ_M and $\chi_M T$ below 42 K and the very large $\chi_M T$ maximum suggest that there is a mechanism of generating uncompensated spin moments and that an F-like correlation between the uncompensated spins is operative and develops into long-range F ordering. The final rapid drop in $\chi_M T$ below 19 K may be due to saturation effects.

To evaluate the AF interaction (J) mediated by the EE azido bridges, we simulated the experimental data above 42 K using the expression derived by Lines for an $S = {}^5/_2$ AF quadratic layer based on the Hamiltonian $\mathbf{H} = -J\sum\mathbf{S}_i\mathbf{S}_j$ ($\mathbf{S}$ sums all pairs of nearest-neighbor spins i and j):[37]

$$\chi_M = Ng^2\beta^2/[|J|(3 + 4 + 1.448\theta^{-1} + 0.228\theta^{-2} + 0.262\theta^{-3} + 0.119\theta^{-4} + 0.017\theta^{-5})] \quad (4)$$

where $\theta = kT/[|J|S(S + 1)]$ with $S = {}^5/_2$. With g fixed at 2.00, the simulation leads to $J = -2.5$ cm^{-1}. This value is comparable with those for the related 2D Mn(II) compounds reported elsewhere (2.24−3.83 cm^{-1}).[7c,9,26] The experimental data above 42 K can also be satisfactorily simulated by means of the analytical expression derived by Curély for an infinite 2D square lattice of classical spins:[38]

$$\chi_M = [Ng^2\beta^2S(S + 1)/3kT][(1 + u)^2/(1 - u)^2] \quad (5)$$

where u is the Langevin function defined above. The best fit with g fixed at 2.00 leads to $J = -2.4$ cm^{-1}, which is very close to the value derived from the Lines expression.

The uncompensated spin moment and ferromagnetism of **3** at low temperature is attributable to spin canting within the AF layers and the long-range ordering of the spin-canted state. The occurrence of spin canting is consistent with the systematic alternation of two different orientations of the coordination polyhedrons throughout the layer. To further characterize the magnetic transition, FC and ZFC magnetization measurements were performed at different fields (Figure 11). The field dependence of the FC magnetization curves is evident. Upon cooling, the FC magnetization at 200 G increases rapidly below 42 K to reach a sharp maximum at 22 K and then drops rapidly. This suggests the onset of an AF transition, which may be due to weak 3D AF ordering of the spin-canted layers. However, the FC magnetization at 300 G or above shows no maximum and tends to saturate

(35) Shen, Z.; Zuo, J. L.; Yu, Z.; Zhang, Y.; Bai, J. F.; Che, C. M.; Fun, H. K.; Vittal, J. J.; You, X. Z. *J. Chem. Soc., Dalton Trans*. **1999**, 3393−3398.
(36) Cortés, R.; Drillon, M.; Solans, X.; Lezama, L.; Rojo, T. *Inorg. Chem*. **1997**, *36*, 677−683.
(37) Lines, M. E. *J. Phys. Chem. Solids* **1970**, *31*, 101−116.
(38) (a) Curély, J. *Europhys. Lett.* **1995**, *32*, 529−543. (b) Curély, J. *Physica B* **1998**, *254*, 277−297. (c) Dalai, S.; Mukherjee, P. S.; Zangrando, E.; Chaudhuri, N. R. *New J. Chem*. **2002**, *26*, 1185−1189.

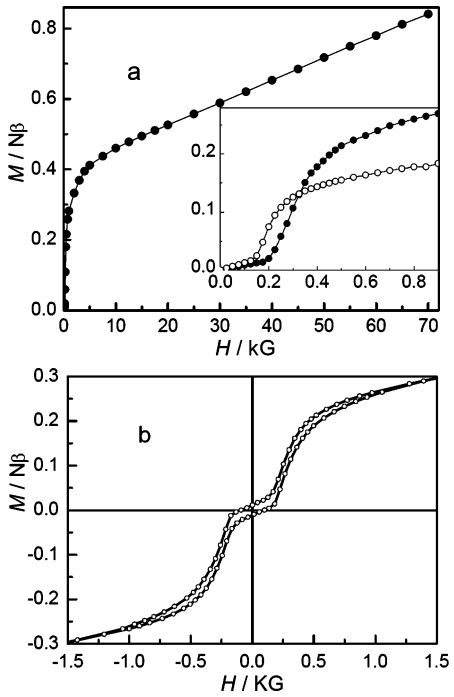

Figure 12. (a) Magnetization from 0 to 70 kG at 1.8 K. The inset shows the low-field parts of the magnetization curves at 1.8 (filled circles) and 22 K (open circles). (b) Hysteresis loop of **3** at 1.8 K.

at lower temperatures, indicating that the weak interlayer AF interaction is overcome by the external field to result in an ordered F phase. These features are indicative of a field-induced metamagnet. The ZFC magnetization curve measured under 300 G diverges from the FC curve below about 23 K, confirming the onset of long-range F ordering under the field.

The magnetization vs field plots confirm that complex **3** is a metamagnet built of spin-canted AF layers (Figure 12). The magnetization at 1.8 K first increases slowly with the field, as for a typical antiferromagnet, and then increases abruptly above 200 G, indicating the onset of the field-induced spin-flop transition from the AF phase to an F phase. The critical field, estimated as the field at which $\partial M/\partial H$ reaches a maximum, is ca. 300 G. Upon a further increase in the field above the critical field, the magnetization increases more and more slowly as the F phase tends to saturate, and finally a linear M vs H relationship is achieved above 9 kG. The magnetization (0.84 Nβ) reached at 70 kG is far below the saturation value (5 Nβ) expected for an $S = {}^5/_2$ system, consistent with the AF nature of the interaction between neighboring Mn(II) ions. The magnetization curve at 22 K also exhibits the sigmoidal shape, but the AF to F transition occurs at a lower field (H_c = 180 G), which is typical of a metamagnet. The hysteresis loop measured at 1.8 K also shows the typical sigmoidal shape, with a remnant magnetization of 0.011 Nβ and a coercive field of 90 G. The existence of the remnant magnetization at a zero field suggests that the F state induced by a higher field is metastable in the absence of a magnetic field. Extrapolating the high-field linear part of the magnetization curve at 1.8 K to zero field gives a magnetization value of 0.40 Nβ, from which the spin-canting angle was estimated to be about 4.6°.[32] This canting angle is the largest of the values ever reported for weak ferromagnets with azido bridges, consistent with the very large $\chi_M T$ maximum observed in Figure 10.

It is worthwhile to compare the magnetic behaviors of **3** and the compounds containing similar single EE azido-bridged Mn(II) layers. As we shall see, the comparison demonstrates the great potential of tuning the bulk magnetic properties of the 3D pillared systems by changing organic linkers. The 3D complex with pzdo as pillars is a 3D antiferromagnet (T_N = 62 K) that exhibits spin-flop behavior at low temperature (H_c = 35−42 kG),[13] while the other previous 3D complex (pym as pillars) exhibits weak F ordering due to spin canting (T_c = 50 K).[10] The differences in magnetic behaviors for these complexes may be justified as follows. In the pzdo and pym compounds, the short interlayer Mn···Mn distances, which are comparable with the intralayer distances, suggest that the interlayer AF interactions are much stronger compared to those in **3**. In the pym compound, the nearest Mn(II) coordination spheres from neighboring layers have different orientations due to the angular coordination of pym, so spin canting may also occur between the Mn(II) ions from different layers. The occurrence of the interlayer spin canting, collaborating with the intralayer one, may justify the observation that the magnetic ordering occurs at a higher temperature than that for **3**. In the pzdo compounds, the feature that the nearest Mn(II) coordination spheres from neighboring layers have the same orientation avoids the interlay spin canting, and the intra- and interlayer isotropic interactions collaborate to give rise to 3D AF ordering at a relatively high temperature. The observation that the spin-flop transition for the pzdo compound occurs at much higher field than that for **3** clearly confirms that the interlayer AF interaction in the former is much stronger than that in the latter. Perhaps the intralayer spin canting in the former compound is depressed by the interlayer interaction. Of the three known 2D compounds, only $[Mn(4\text{-acpy})_2(N_3)_2]_n$ was found to exhibit ferromagnetism due to spin canting (T_c = 28 K; metamagnetic behaviors cannot be excluded because field-variable magnetic measurements were not reported).[26a] The absence of spin canting in $[Mn(DENA)_2(N_3)_2]_n$ has been attributed to the nearly parallel arrangement of neighboring coordination polyhedra.[7c] For the third compound, $[Mn(minc)_2(N_3)_2]_n$,[26b] it was suggested that spin canting may occur at $T_c < 2$ K because of the relatively weaker intralayer interaction (J = 2.24 cm^{-1}).[7c]

(d) Complex 4. The temperature dependence of magnetic susceptibility (χ_M) for compound **4** is shown in Figure 13. The $\chi_M T$ value per Mn(II) at 300 K is 3.84 emu K mol^{-1}, also lower than the spin-only value for a magnetically isolated Mn(II) system. Upon cooling, $\chi_M T$ decreases but χ_M increases in the whole temperature range from 300 to 2 K. The increase of χ_M is very slow from 35 to 14 K but becomes more and more rapid upon further cooling.

The decrease of $\chi_M T$ indicates that an AF interaction is operative between neighboring Mn(II) ions. According to the structural data, compound **4** is a 2D compound in which single EE azido-bridged 1D chains are interlinked by organic

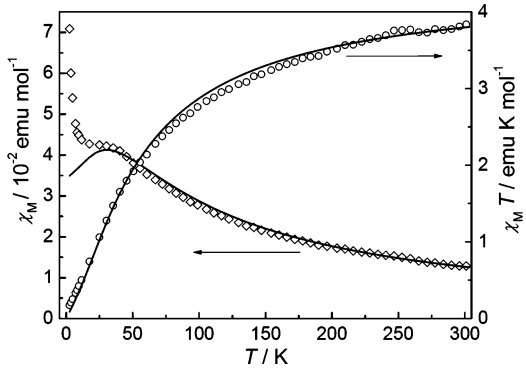

Figure 13. Temperature dependences of χ_M and $\chi_M T$ for **4**. The solid lines are drawn in the whole temperature range from the parameters obtained by fitting the experimental data above 25 K to eq 1.

ligands. The magnetic exchange through the long organic bridge should be negligible, so the AF interaction should be mainly through the single EE azido bridge to give AF chains. The susceptibility of a typical AF Mn(II) chain should exhibit a maximum at certain temperatures, below which a smooth decrease occurs, as observed for Mn(II) chains with uniform double EE azido bridges or with alternating double EE and double EO azido bridges (see Figure 9 for compound **2**). Although **4** exhibits no maximum in χ_M, the shape of the χ_M vs T plot suggests that the maximum should be between 35 and 20 K and may be obscured by the increase of χ_M in the low-temperature range. To evaluate the interaction (J) via the single EE azido bridge, we tried to simulate the experimental data by means of the Fisher equation for the $S = {}^5/_2$ uniform chain (eq 1). With g fixed at 2.0, the best fit of the experimental data above 25 K led to $J = -5.1$ cm^{-1}. The solid lines in Figure 7 represent the susceptibility calculated in the whole temperature range with the above parameter. As can be seen, the agreement between the experimental and fitted data above 32 K is good, and the maximum would appear at about 30 K if it were not obscured.

To characterize the low-temperature increase of χ_M, we have performed low-field FC and ZFC magnetization measurements for **4** below 30 K. Upon cooling from 30 to 2 K, the magnetization (and χ_M) increases rapidly but exhibits no abrupt transition and the $\chi_M T$ product decreases quasi-linearly. This suggests that no spontaneous magnetization occurs in the temperature range measured. The absence of long-range ordering is also confirmed by FC and ZFC magnetization data, which showed no difference in the whole temperature range. Such a low-temperature behavior is different from the behaviors of **1** and **3**, where the low-temperature increase in χ_M is accompanied by long-range ordering.

The low-temperature increase of χ_M in AF systems was often attributed to the presence of a certain amount of paramagnetic impurities. Following this line, we simulated the experimental data of **4** to the following equation over the whole 2−300 K temperature range:

$$\chi_M = \chi_{chain}(1 - \rho) + [Ng^2\beta^2S(S + 1)/3kT]\rho \qquad (6)$$

where χ_{chain} is defined by the Fisher equation (1) and ρ is the amount of the paramagnetic impurities [presumably a mononuclear Mn(II) complex]. The least-squares fit with g fixed at 2.0 reproduces the experimental data quite well in the whole temperature range, leading to $J = -5.3$ cm^{-1} and $\rho = 2.2\%$. This J value is similar to that obtained above without taking into account the low-temperature data.

Extended Hückel molecular orbital calculations showed that the magnetic interaction between Mn(II) ions bridged by the EE azido ion should always be AF and that the AF interactions should maximize as the Mn−N−N bond angle approaches 110° and the Mn−N_3−Mn torsion angle approaches 0 or 180°.[9] Compared with the previous Mn(II) chain with single EE azido bridges in trans positions ($J = -4.8$ cm^{-1}),[30] the larger Mn−N−N bond angles for **4** (136.0 and 155.9° vs 125.2 and 118.8°) favor a weaker interaction but the much smaller Mn−N_3−Mn torsion angle of **4** (0.7° vs 126.8°) suggests a stronger interaction. It is likely that the influence of the torsion angle dominates, resulting in the slightly stronger interaction in **4**. Following this trend, the single azido bridge in **3**, where the Mn−N−N angles (146.1 and 128.6°) are comparable but the torsion angle (94.6°) is very close to 90°, propagates a significantly weaker interaction ($J = -2.5$ cm^{-1}). However, this trend seems invalid when taking into account the known Mn(II) chain with single EE azido bridges in cis positions,[16a] for which two J values, −3.5 and −0.12 cm^{-1}, were estimated for the alternating bridges with the same torsion angle (180°) but with different Mn−N−N angles (127.6 and 159.8°, respectively).

The successful fit of the low-temperature increase in χ_M to eq 6 confirms the absence of long-range ordering, but it does not warrant that the paramagnetic impurities are really at the origin of the χ_M increase. An alternative origin may be spin canting. Although spin canting often provokes long-range magnetic ordering, as observed for **1**, **3**, and related systems, long-range magnetic ordering, in principle, is not an obligatory consequence of spin canting. Along the azido-bridged chain in **4**, the coordination polyhedra are systematically slanted toward different directions because of the lack of inversion centers within the chain. This may lead to spin canting within the manganese(II) azido chains, and perhaps because of the lack of appropriate interchain correlations, the long-range ordering of the canted spins is not achieved at $T \geq 2$ K. It seems to us that neither the paramagnetic impurities nor the spin canting can be warranted or excluded based on the present experimental data. To better understand the real origin of the low-temperature magnetic behavior, neutron diffraction studies may be needed.

Conclusion

Four new inorganic−organic hybrid coordination polymers in which 1D or 2D manganese(II) azido inorganic motifs are interlinked into higher-dimensional networks by organic linkers have been synthesized by use of a series of bis(pyridyl)-type organic bridging ligands (linkers) with different side groups and/or different coordination orientations. The dimensionality and the topology of the manganese(II) azido motif and the whole structure are sensitive to the organic linkers used. Compounds **1** and **3** are 3D pillared-

layer architectures: **1** is the first 3D network built by pillaring 2D Mn(II) layers of alternate double EO and single EE azido bridges, and **3** is built from single EE azido-bridged Mn(II) layers, with a novel 3D net topology. The 3D nets of **1**, **3**, and related compounds have been related to the specific length and coordination orientation of the organic pillars, and the undulated shape of the manganese(II) azido layers. Consistent with their structures, both **1** and **3** exhibit weak ferromagnetism due to spin canting. Compound **1** is a weak ferromagnet with $T_c = 16$ K, and **3** is a metamagnet with $T_c = 23$ K. On the other hand, compounds **2** and **4** are 2D coordination networks in which 1D manganese(II) azido chains are interlinked by the organic linkers: **2** is the first 2D network built from Mn(II) chains with alternate double EE and double EO azido bridges, which mediate AF and F interactions, respectively; **4** is the first 2D network built from Mn(II) chains with only single EE azido bridges, which mediate AF interactions.

This contribution demonstrates the great potential of designing new metal azido based materials with interesting 3D networks and magnetic properties. By rational design of the organic linkers with different length and/or different coordination orientations, we should be able to tune the network topology, interlayer, or interchain magnetic interactions and hence the bulk magnetic properties of the materials.

Acknowledgment. We are thankful for the financial support from NSFC (Grants 20201009 and 20490210), the Foundation of Science and Technology Development of Shanghai (Grant 03ZR14024), and the "Shuguang" Project founded by Shanghai Municipal Education Commission and Shanghai Education Development Foundation (Grant 04SG28).

Supporting Information Available: Crystallographic data (CIF) for compounds **1**−**4**. This material is available free of charge via the Internet at http://pubs.acs.org.

IC0512328